

Search method for unmodeled transient gravitational waves associated with SGR flares

Abstract.

We describe a method for searching for transient gravitational waves associated with Soft Gamma-ray Repeater flares or other burst-like events using data collected by interferometric gravitational wave detectors. The method as implemented can be used to analyze data from either a single detector or from two detectors coherently. The excess power type algorithm creates a time series from conditioned detector data which is then calibrated via signal simulations of known strength based on plausible waveform classes. Estimated search sensitivities obtained by performing two-detector searches on simulated S5 LIGO data are presented. In the case of 22 ms duration white noise bursts in the 100-200 Hz band, we find characteristic strain sensitivity $h_{\text{rss}}^{90\%} = 2.8 \times 10^{-22} \text{ Hz}^{-\frac{1}{2}}$.

PACS numbers: 07.05.Kf

P. Kalmus, S. Márka, L. Matone, R. Khan

Columbia University, New York, NY 10027, USA

E-mail: peter.kalmus@ligo.org

1. Introduction

Soft Gamma-ray Repeaters (SGRs) are objects in the sky which sporadically emit brief (< 0.2 s) energetic soft gamma-ray bursts. Common bursts have detected peak luminosities of up to 10^{43} erg/s (assuming isotropic emission) and rare ‘giant flare’ events can have detected peak luminosities of up to 10^{47} erg/s [1]. Of the four confirmed SGRs, three have produced a giant flare since their discovery in 1979 [2–4].

One explanation for this class of objects (and the similar ‘Anomalous X-Ray Pulsars’) is provided by the ‘magnetar’ model [5; 6]. Magnetars are believed to be neutron stars with the strongest magnetic fields in the Universe, $\sim 10^{14} - 10^{15}$ G [4; 5]. In this model SGR bursts are explained by interaction of the star’s magnetic field and solid crust, leading to bending and stretching of the crust and occasional catastrophic crustal cracking resulting in a giant flare [7; 8]. Another competing explanation is that SGRs are quark stars with bursts driven by ‘starquakes’ [9–12]. In any case, the possibility of reconfiguration of star matter during giant flares make SGRs interesting candidates for gravitational wave (GW) emission.

We present a search method for GW transients associated with triggered bursts using data collected by GW detectors such as LIGO [13]. The method was developed for SGR flare searches, but it could be used to search for GWs associated with most burst-like triggers.

The search targets unmodeled transient GW signals which may be emitted at the moment of crustal rearrangement. To preserve generality we make no assumptions about SGR models beyond approximate coincidence of the light curve features and GW peak times and durations. We focus primarily on band-limited white noise bursts (WNBs) as the most general albeit not directly astrophysically motivated waveforms. For SGR flare searches WNB durations are set by timescales in flare light curves, and frequency bands are set by the detector’s sensitive region. In this paper, we first present our search method then estimate its sensitivity to example target signal classes in simulated LIGO noise.

2. Method

In this section we give a description of the search pipeline, an excess power type search [14–16] using loudest event statistics to estimate upper limits [17]. We consider the pipeline (Fig. 1) at two levels: high-level overviews of search, upper limit estimation, and sensitivity estimate overviews; and the core data processing algorithm which converts raw detector data into a measure of excess power (or ‘cross excess power’ in the two-detector case).

2.1. Search overview

In a search on real data, the pipeline can be used to search for GW candidates or to estimate upper limits using data from GW detectors. We divide available detector data

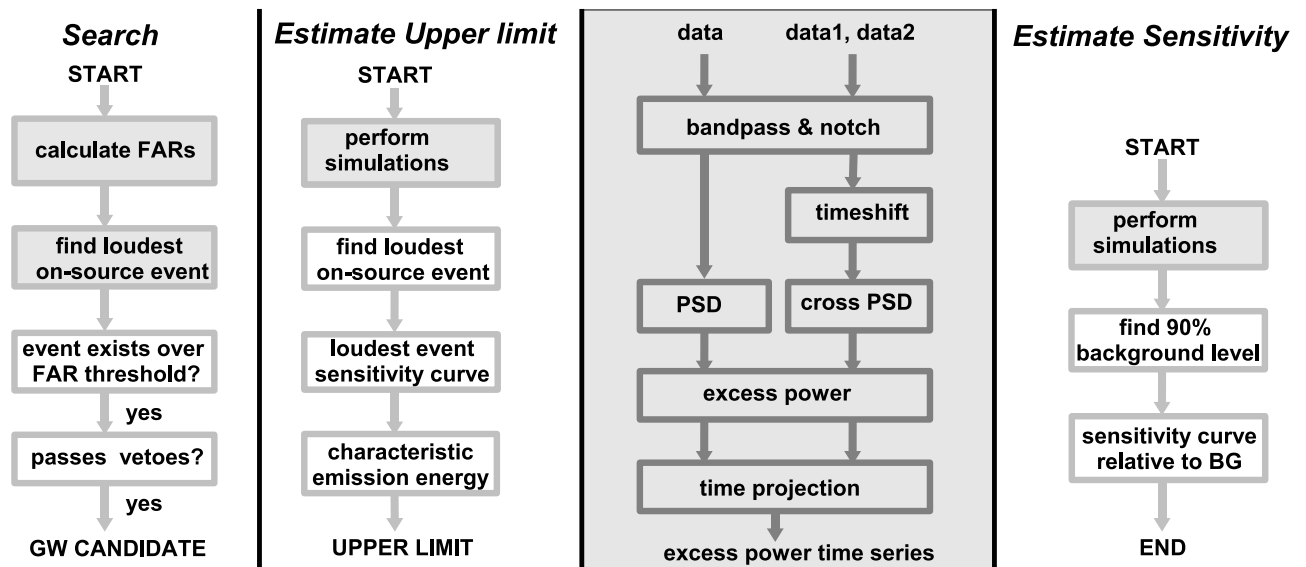


Figure 1. Diagrams of the pipeline. On the left are diagrams illustrating the search for GW candidates and upper limit estimation carried out in a search on real data. On the right is a diagram illustrating sensitivity estimation carried out on simulated data (Section 3). The central shaded region diagrams data processing steps (Section 2.2). Shaded boxes are steps in which the data processing algorithm is applied.

into an on-source region in which we might expect to find the GW signal associated with the astrophysical trigger, and an off-source region which provides a background for the search. The off-source region is chosen close enough to the on-source region to ensure similar detector behavior. We first estimate false alarm rates (FARs) from the off-source region, and compare the loudest on-source event to a pre-determined FAR detection threshold, set so that we expect no more than one false detection in 100 years of sky observation. (This corresponds to much less than 100 years of data since we analyze small regions of data around rare astrophysical triggers.) Events above this threshold, if any, are subject to environmental channel vetoes and waveform consistency checks.

We can also estimate upper limits on GW strain at the Earth via simulated signals injected into the raw data (Section 2.3.) The on-source loudest event is used as a threshold for creating a sensitivity curve from the simulations. (This upper limit threshold is unrelated to the detection threshold mentioned in the previous paragraph.)

In the case of simulated detector data we estimate search sensitivity. The steps are identical to those used for estimating an upper limit except the sensitivity curve is constructed from a measure set relative to noise events instead of to a loudest on-source event (Section 3.1).

2.2. Data processing

Data processing takes as input either a single stream of raw detector data or two synchronized (or time-shifted) streams from two detectors. It produces as output an excess power type time series (one detector) or a ‘cross excess power’ time series (two detectors).

First, data is conditioned via digital filters. For a two-detector search a time delay is applied as appropriate for the relative locations of astrophysical source and GW detectors. Next, the power spectral density (PSD) or cross PSD is calculated. Then the mean PSD value from off-source data at each frequency bin is subtracted from elements of that frequency bin to estimate excess power; this has an effect similar to whitening procedures. Finally, a time series is created by projection onto the time axis.

2.2.1. Data conditioning Data conditioning consists of zero-phase digital filtering in the time domain [18], first with a bandpass filter and then with a composite notch filter.

The basic IIR bandpass filter’s passband is set by the detectors’ all-inclusive sensitive band (64-2048 Hz for LIGO detectors). A single bandpass filter is used for all searches.

The notch filter is created using off-source ‘training data’. Long duration narrow band signals are not targeted by our search and their removal in the time domain maximizes the useful bandwidth of the search. We remove narrow lines associated with the power line harmonics at multiples of 60 Hz, the violin modes of the mirror suspension wires, calibration lines, and narrow band noise sources of unknown origin. In a two-detector search, lines are found separately for each detector’s data stream, and the union of both sets of lines are used to create a single notch filter.

A buffer interval of 5 seconds on each side of filtered data is discarded. This buffer is significantly longer than the characteristic impulse and step response of the filters.

2.2.2. Measuring excess power We next create a time-frequency tiling (spectrogram) from the conditioned input data stream(s). This is a series of windowed (Blackman) discrete fourier transforms, of time length δt set by the target signal duration. Each tiling column corresponds to a time bin of width δt and each row corresponds to a frequency bin of width δf , both linearly spaced, with $\delta f \delta t = 1$. Adjacent time bins overlap by $0.9\delta t$ to guard against mismatch between prospective signals and tiling time bins. Larger overlaps require more computation and do not noticeably improve sensitivity.

In a one-detector search, we then have a complex-valued time-frequency tiling from which we calculate the real-valued one-sided PSD for every time bin. To do this we multiply each tile value by its complex conjugate and normalize the result (accounting for sampling frequency and windowing function). We then discard frequency bins outside of the chosen search band.

In a two-detector search, we have two complex time-frequency tilings, one for each

detector, from which we calculate

$$T_{ij}^{\text{dual}} = T_{ij}^{(1)} * T_{ij}^{(2)*}, \quad (2.1)$$

where T represents a tiling matrix and i and j are frequency and time bin indices, and (1) and (2) denote the detector. The real part is kept, and normalization is applied as in the one-detector case. To obtain a positive-definite estimator we next take the absolute value of each tile; this allows sensitivity to both strongly correlated and strongly anti-correlated signals in the two (potentially misaligned) detectors.

Next, we remove the background noise power from each element of the PSD time-frequency tiling, using off-source data. A measure of the signal excess power remains. We choose to measure noise power using the mean from a gamma distribution, which provides a good fit in both one and two-detector cases; other measures may be preferred when working with real detector data. At a given frequency bin (row), we first randomly select a subset of elements to eliminate artifacts. The selection density is set by the half width of the autocorrelation central peak and the target signal duration (i.e. no overlap allowed). The selected elements are fit to a gamma distribution, and outliers above a threshold (typically four standard deviations) are discarded. This process repeats until no outliers remain. The resulting estimate on the mean is subtracted from each element of the corresponding frequency bin in the PSD matrix, giving a matrix of excess power (or ‘cross excess power’ in the two-detector case).

To create a time series out of the excess power matrix, we project onto the time axis. For wide-band target signals we include all frequency bins within the search band in the projection. For monochromatic target signals we take the two loudest adjacent frequency tiles in every time bin. Taking two tiles instead of one guards against mismatch between tiling frequency bin boundaries and signal location.

2.3. Simulations

GWs have two independent polarization states $h_+(t)$ and $h_\times(t)$. The magnitude of the response excited in an interferometric detector by a passing wave depends on the direction from which the wave arrives relative to the detector, and its polarization state, and is customarily described by the ‘antenna functions’ $F^+(\theta, \phi, \psi)$ and $F^\times(\theta, \phi, \psi)$. Here θ is the altitude of the source relative to the detector’s horizon, ϕ is the azimuth of the source relative to the detector’s x-arm, and ψ is the polarization angle. (In a triggered search the source location is well-known.)

Our goal is to simulate incoming GWs chosen from the ‘signal space.’ The pipeline measures the detector output $h_d(t)$, consisting of the detector signal response $\xi_d(t)$ in the presence of detector noise $n_d(t)$ (assuming a perfectly calibrated detector):

$$h_d(t) = n_d(t) + \xi_d(t), \quad (2.2)$$

where $\xi_d(t)$ is given by

$$\xi_d(t) = F_d^+(\theta, \phi, \psi)h_+(t) + F_d^\times(\theta, \phi, \psi)h_\times(t), \quad (2.3)$$

and the antenna functions are given by

$$F_d^+(\theta, \phi, \psi) = \frac{1}{2} \cos 2\psi (1 + \cos^2 \theta) \cos 2\phi - \sin 2\psi \cos \theta \sin 2\phi \quad (2.4)$$

$$F_d^\times(\theta, \phi, \psi) = -\frac{1}{2} \sin 2\psi (1 + \cos^2 \theta) \cos 2\phi - \cos 2\psi \cos \theta \sin 2\phi. \quad (2.5)$$

We simulate a detector response $\xi_d(t)$ by first generating waveforms h_+^{sim} and h_\times^{sim} . In the examples presented in Section 3 the energy in h_+^{sim} and h_\times^{sim} is chosen to be the same, where the energy in a localized discrete signal $h(t)$ is defined as

$$h_{\text{rss}}^2 = \frac{1}{f_s} \sum_i h_i^2, \quad (2.6)$$

where f_s is the sampling frequency and i is the discrete time index.

For some polarization angle ψ we calculate the antenna factors $F_d^+(\theta, \phi, \psi)$ and $F_d^\times(\theta, \phi, \psi)$, and explicitly construct the detector response $\xi_d(t)$. This simulated signal is then injected into the noise at randomly chosen time locations in the off-source region. In a two-detector search this process is performed for each detector, with identical simulated signals h_+^{sim} and h_\times^{sim} and polarization angle ψ .

We recover the loudest event in a time window (with length set by the on-source region) around each injected simulation. We repeat this process with a range of simulation energies in order to determine the pipeline's response (Fig. 2).

3. Sensitivity

3.1. Measuring sensitivity

When running the search pipeline on real data we choose a sensitivity curve threshold equal to the loudest on-source event (Section 2.1). With simulated data we desire a sensitivity curve threshold set relative to the noise (Fig. 2). We divide a long stretch of processed data into shorter segments (of a length equal to a simulated 'on-source' region of 2 s) and choose the loudest event from each segment. We then take the level corresponding to the 90th percentile of this collection as the sensitivity curve threshold.

For every injected simulation, we determine whether an event exists above this threshold in the 2 s long time window surrounding the injection (e.g. Fig. 2(a)). If there is such an event, which may be due either to the injected simulation or a noise peak (false alarm), a value of 1 is recorded at the simulation h_{rss} value; if not a value of 0 is recorded. The sensitivity curve describing detection efficiency vs. h_{rss} is given by fitting to $f_{\text{sigmoid}}(x) = 1 / (1 + e^{-\alpha(x-\beta)})$ [19] where α and β are fit parameters (Fig. 2(b)). At a fraction detected of 0.9, false alarm levels are less than $\sim 10^{-7}$ Hz and thus contribute negligibly to the $h_{\text{rss}}^{90\%}$ value.

3.2. Example results of two-detector searches

We present sensitivity estimates for simulated data with noise PSD matched to real LIGO data (H1 and L1 detectors on 2005 Dec 02, during the 5th science run), for three

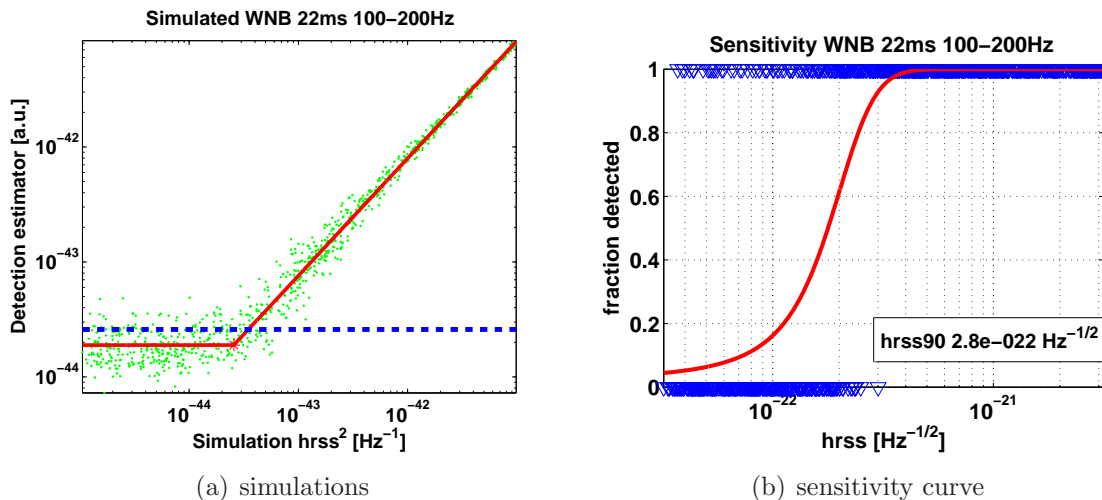


Figure 2. (a) Example plot of injected vs. recovered signal strengths (22 ms duration WNBs). Simulations were injected into simulated noise and the two-detector algorithm was used. Each point represents the loudest event recovered from a region surrounding an injection whose length is the same as the on-source region. At very high energies the loudest event is likely due to the simulation. At very low energies the simulations are lost in the noise and the loudest event is likely due to a local noise peak. The dotted line indicates the threshold used in constructing a sensitivity curve. (b) Example sensitivity curve. Each triangle in the plot answers ‘was there an event above threshold in the window surrounding the injection?’ These 0 or 1 responses are fit to create the efficiency curve.

example target signal classes: 22 ms duration WNBs between 100 and 200 Hz; 100 ms duration WNBs between 64 and 1024 Hz; and neutron star ringdown (RD) waveforms with time constant $\tau = 150$ ms at 1900 Hz. We expect some performance degradation when running on real data, which may contain non-stationarities and phase relationships not present in simulated data. Search bands for the WNB searches were chosen to match the detectors’ sensitive region. RD waveforms between $\sim 1 - 2$ kHz (we choose a search band between 1 and 2 kHz) are predicted GW signals in some SGR flare models [20–22]. We note that for the case of RD waveforms we do not expect our search to perform as well as a matched filtering search [23].

Searches were run as they would be run for a real event, using the celestial coordinates of SGR 1806-20 and a simulated trigger time chosen to give optimal source location relative to the LIGO detectors. FARs depend on vetoes and waveform consistency cuts and are not presented here.

3.2.1. 22 ms WNBs between 100 Hz and 200 Hz This search targeted narrow-band WNBs limited to between 100-200 Hz, with 22 ms duration (Table 1).

We choose to impose two constraints on the h_+ and h_\times polarization components of this example signal class: equal energy, and an absolute cross-correlation between polarization components of less than 0.1 (where maximum correlation is +1 and

Table 1. Two-detector search sensitivity estimates (strain/ \sqrt{Hz}) for target signal classes mentioned in the text, for searches that do not depend on polarization angle. Ringdown (RD) searches in the table are for circularly polarized simulations. 90% confidence strain sensitivities are given. These values are averages of 30 trials with different values of ψ ; 90% confidence statistical uncertainty is $\sim 1\%$. The searches were performed on simulated data.

target signal	$h_{rss}^{90\%}$
WNB 22ms 100-200Hz	2.79e-22
WNB 100ms 64-1024Hz	1.05e-21
RD 150ms 1900Hz	1.72e-21

maximum anti-correlation is -1). If no cross-correlation constraint is imposed, search sensitivity to relatively narrow-band white noise bursts shows a ψ -dependence. This can be understood with the observation that band-limited WNB simulations approach sine-Gaussian waveforms as the allowed bandwidth approaches zero. The distribution in cross-correlation between h_+ and h_\times becomes wider as simulations approach pairs of sine-Gaussian-like signals with an undetermined relative phase.

3.2.2. 100 ms WNBs between 64 Hz and 1024 Hz This search targeted relatively broad-band WNBs between 64 and 1024 Hz, with 100 ms duration (Table 1).

As before, we choose to impose a constraint that h_+ and h_\times carry equal energy. In this case there is no need to impose a constraint on the cross-correlation between h_+ and h_\times , since the distribution in cross-correlation is already sharply peaked around zero.

3.2.3. Neutron star ringdown waveforms with $\tau = 150$ ms The target signal class for this search were $\tau = 150$ ms ringdowns. We present results for both linearly and circularly polarized ringdowns at 1900 Hz (Fig. 3, Table 1). Fig. 3 represents several sensitivity curves over one period ($\pi/2$) in polarization angle ψ . Variation over polarization angle is evident in the linearly polarized case only; we do not expect ψ -dependence in the circular case because the h_+, h_\times cross-correlation is zero.

4. Conclusion

We have described a search method targeting unmodeled transient GWs which may be emitted during SGR flare events or other burst events. The search can be run either on data from a single interferometric GW detector, or coherently on simultaneous data from two detectors.

We have presented sensitivity estimates for three classes of target signals. In the case of 22 ms duration white noise bursts in the 100-200 Hz band, we find a characteristic strain sensitivity $h_{rss}^{90\%} = 2.8 \times 10^{-22} \text{ Hz}^{-\frac{1}{2}}$.

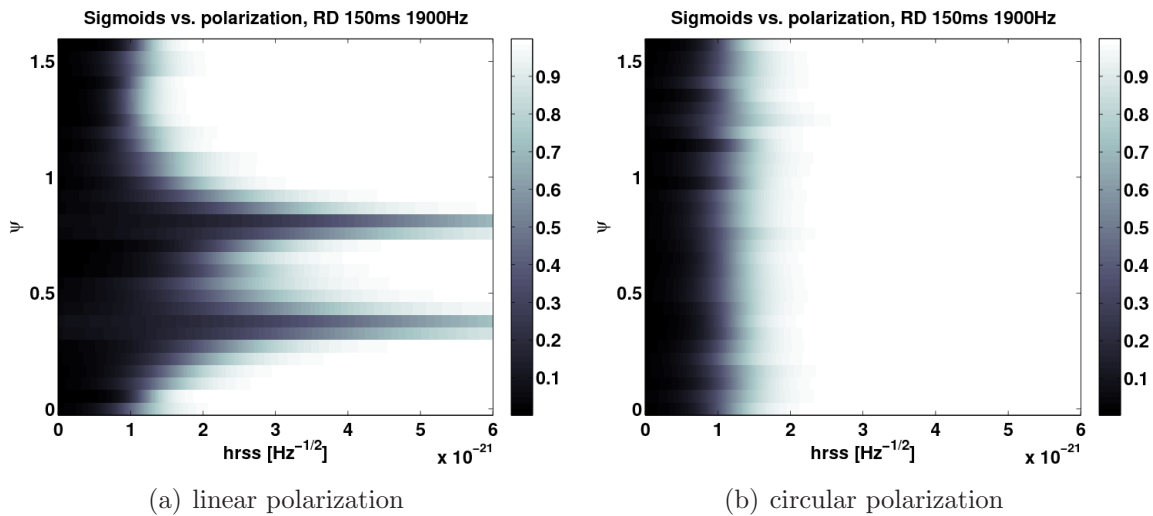


Figure 3. Sensitivity curves from two-detector simulated data search for neutron star ringdown (RD) waveforms at 1900 Hz with linear polarization (a) and circular polarization (b) as a function of polarization angle ψ . Each horizontal stripe in the figure can be thought of as the top view of a sensitivity curve (e.g. Fig. 2 (b)). The grayscale depth represents fraction detected. The sensitivity minimum in (a) at $\psi \simeq 0.3$ corresponds to the LIGO Hanford antenna pattern minimum, and the minimum at $\psi \simeq 0.8$ corresponds to the LIGO Livingston antenna pattern minimum.

Acknowledgment

The authors are grateful for the support of the United States National Science Foundation under cooperative agreement PHY-04-57528 and Columbia University in the City of New York. We are grateful to the LIGO collaboration for their support. We are indebted to many of our colleagues for helpful discussion, in particular Z. Márka. The authors gratefully acknowledge the support of the United States National Science Foundation for the construction and operation of the LIGO Laboratory and the Particle Physics and Astronomy Research Council of the United Kingdom, the Max-Planck-Society and the State of Niedersachsen/Germany for support of the construction and operation of the GEO600 detector. The authors also gratefully acknowledge the support of the research by these agencies and by the Australian Research Council, the Natural Sciences and Engineering Research Council of Canada, the Council of Scientific and Industrial Research of India, the Department of Science and Technology of India, the Spanish Ministerio de Educacion y Ciencia, The National Aeronautics and Space Administration, the John Simon Guggenheim Foundation, the Alexander von Humboldt Foundation, the Leverhulme Trust, the David and Lucile Packard Foundation, the Research Corporation, and the Alfred P. Sloan Foundation. This paper has been assigned LIGO Document Number LIGO-P070024-00-Z.

References

- [1] Woods P M and Thompson C 2004 in W G H Lewin and M van der Klis, eds, *Compact Stellar X-Ray Sources* (Cambridge: Cambridge Univ. Press) (*Preprint astro-ph/0406133*)
- [2] Mazets E P *et al.* 1979 *Nature* **282** 587–589
- [3] Hurley K *et al.* 1999 *Nature* **397** 41–43 (*Preprint astro-ph/9811443*)
- [4] Hurley K *et al.* 2005 *Nature* **434** 1098–1103 (*Preprint astro-ph/0502329*)
- [5] Duncan R C and Thompson C 1992 *Astrophys. J. Lett.* **392** L9–L13
- [6] Thompson C and Duncan R C 1995 *MNRAS* **275** 255–300
- [7] Schwartz S J, Zane S, Wilson R J, Pijpers F P, Moore D R, Kataria D O, Horbury T S, Fazakerley A N and Cargill P J 2005 *Astrophys. J. Lett.* **627** L129–L132 (*Preprint astro-ph/0504056*)
- [8] Palmer D M *et al.* 2005 *Nature* **434** 1107–1109 (*Preprint astro-ph/0503030*)
- [9] Xu R X 2003 *Astrophys. J. Lett.* **596** L59–L62 (*Preprint astro-ph/0302165*)
- [10] Owen B J 2005 *Physical Review Letters* **95**(21) 211101–+ (*Preprint astro-ph/0503399*)
- [11] Xu R X, Tao D J and Yang Y 2006 *Mon. Not. R. Astr. Soc.* **373** L85–L89 (*Preprint astro-ph/0607106*)
- [12] Horvath J E 2005 *Modern Physics Letters A* **20** 2799–2804
- [13] Hughes S A, Marka S, Bender P L and Hogan C J 2001 *ECONF C* **010630** 402
- [14] Flanagan É É and Hughes S A 1998 *Phys. Rev. D* **57** 4535–4565 (*Preprint gr-qc/9701039*)
- [15] Flanagan É É and Hughes S A 1998 *Phys. Rev. D* **57** 4566–4587 (*Preprint gr-qc/9710129*)
- [16] Anderson W G, Brady P R, Creighton J D and Flanagan É É 2001 *Phys. Rev. D* **63**(4) 042003–+ (*Preprint gr-qc/0008066*)
- [17] Brady P R, Creighton J D E and Wiseman A G 2004 *ArXiv General Relativity and Quantum Cosmology e-prints* (*Preprint gr-qc/0405044*)
- [18] Hamming R 1998 *Digital Filters* (New York: Dover Publications)
- [19] Kingsland S 1995 *Modeling Nature* (Chicago: University of Chicago Press)
- [20] Andersson N and Kokkotas K D 1998 *Mon. Not. R. Astr. Soc.* **299** 1059–1068 (*Preprint gr-qc/9711088*)
- [21] de Freitas Pacheco J A 1998 *Astronomy and Astrophysics* **336** 397–401 (*Preprint astro-ph/9805321*)
- [22] Ioka K 2001 *Monthly Notices of the RAS* **327** 639–662 (*Preprint astro-ph/0009327*)
- [23] Shawhan P and Ochsner E 2004 *Classical and Quantum Gravity* **21** S1757–S1765 (*Preprint gr-qc/0404064*)